

Oxygen-Barrier Properties of Cold-Drawn Polyesters

R. Y. F. LIU,¹ D. A. SCHIRALDI,² A. HILTNER,¹ E. BAER¹

¹Department of Macromolecular Science, Center for Applied Polymer Research, Case Western Reserve University, 10900 Euclid Avenue, Cleveland, Ohio 44106-7202

²KoSa, 1551 Sha Lane, Spartanburg, South Carolina 29304

Received 15 October 2001; revised 31 January 2002; accepted 5 February 2002

ABSTRACT: The improvement of oxygen-barrier properties of glassy polyesters by orientation was examined. Poly(ethylene terephthalate) (PET), poly(ethylene naphthalate), and a copolymer based on PET in which 55 mol % of the terephthalate was replaced with bibenzoate (PET-BB55) were oriented by constrained uniaxial stretching. In a fairly narrow window of stretching conditions near the glass-transition temperature, it was possible to achieve uniform extension of the polyesters without crystallization or stress whitening. The processes of orientation and densification correlated with the conformational transformation of glycol linkages from gauche to trans. Oxygen permeability, diffusivity, and solubility decreased with the amount of orientation. A linear relationship between the oxygen solubility and polymer specific volume suggested that the cold-drawn polyester could be regarded as a one-phase densified glass. This allowed an analysis of oxygen solubility in accordance with free-volume concepts of gas permeability in glassy polymers. Orientation was seen as the process of decreasing the amount of excess-hole free volume and bringing the nonequilibrium polymer glass closer to the equilibrium (zero-solubility) condition. Cold drawing most effectively reduced the free volume of PET-BB55. © 2002 Wiley Periodicals, Inc. *J Polym Sci Part B: Polym Phys* 40: 862–877, 2002

Keywords: polyesters; poly(ethylene terephthalate); poly(ethylene naphthalate); poly(ethylene terephthalate-co-benzoate); cold drawing; orientation; oxygen diffusion; gas barrier; glassy state; free volume

INTRODUCTION

Orientation significantly improves the oxygen-barrier properties of poly(ethylene terephthalate) (PET).^{1,2} Reduced permeability is achieved even if crystallization is prevented, for example, by orientation below the glass-transition temperature (T_g).³ Usually, the effect of orientation or crystallization in reducing gas permeability is considered in terms of a two-phase model consisting of a permeable phase and an impermeable phase.

However, a two-phase model with constant densities of permeable and impermeable phases often does not give a good correlation with the transport properties of PET. The application of the two-phase model of gas permeability to cold-crystallized PET requires consideration of a dedensified amorphous phase.⁴ Similarly, a two-phase description of gas permeability in cold-drawn and heat-set PET necessitates variable densities of both permeable and impermeable phases.³

The transformation of ethylene linkages from the gauche conformation to the trans conformation during stretching provides the basis for describing transport properties of cold-drawn PET in terms of two phases: a permeable amorphous

Correspondence to: A. Hiltner (E-mail: pah6@po.cwru.edu)

Journal of Polymer Science: Part B: Polymer Physics, Vol. 40, 862–877 (2002)
© 2002 Wiley Periodicals, Inc.

phase with ethylene linkages predominately in the gauche conformation and an impermeable amorphous phase with ethylene linkages that have transformed from gauche to trans during stretching.³ The two-phase concept of cold-drawn PET readily explains heat setting as crystallization and densification of the impermeable amorphous (trans) phase accompanied by dedensification of the permeable amorphous (gauche) phase.

This study tests the formulation of the two-phase model for oriented PET through an examination of the oxygen-transport properties of some other cold-drawn polyesters. Comparisons are made of PET, poly(ethylene naphthalate) (PEN), and a copolymer based on PET in which 55 mol % of the terephthalate is replaced with bibenzoate (PET-BB55). Correlations are sought with the conformation of the ethylene linkage as determined by infrared spectroscopy.

MATERIALS AND METHODS

PET, PEN, and PET-BB55 were supplied as pellets by KoSa (Spartanburg, SC). In addition, a terpolymer based on PET-BB55 was synthesized with 5 or 10% of the terephthalate replaced with isophthalate (PET-BB55/I5 and PET-BB55/I10) to retard crystallization. The procedure for the synthesis has been described in detail elsewhere.⁴ The pellets were dried *in vacuo* at 80 °C for 24 h before molding. The dry pellets were compression-molded and quenched into amorphous films as described previously.⁴ The temperature of the press was 265 °C for PET, 300 °C for PEN, and 290 °C for PET-BB55. A range of film thicknesses of 180–600 μm were prepared. Commercial oriented Vectra films were also tested.

The amorphous films were stretched under constrained uniaxial conditions as described previously.³ The specimen width before stretching was 130 mm, and the thickness and gauge length were varied to achieve a final thickness of 100–200 μm . Grids were marked on the specimen for measuring the draw ratio, and the specimen was clamped between wide grips and mounted in the environmental chamber of an Instron machine. Specimens were drawn at or near T_g . The chosen draw temperatures were high enough to obtain uniform deformation but low enough to avoid crystallization. To obtain barrier specimens that differed in draw ratio but had about the same thickness, we used thinner films and larger gauge lengths for lower draw ratios; thicker films and

smaller gauge lengths were required for higher draw ratios. For example, a PET specimen 400 μm thick with a gauge length of 50 mm was used to obtain a barrier specimen with a draw ratio of about 3, whereas a specimen 600 μm thick with a gauge length of 30 mm was used to obtain a barrier specimen with a draw ratio of about 4. After drawing, the film was rapidly cooled to ambient temperature in the grips by the door of the environmental chamber being opened. The entire process was completed in 2–10 min, depending on the draw rate and draw ratio. Wide-angle X-ray diffraction patterns showed only diffuse amorphous reflections.⁵

A density gradient column was constructed from a solution of calcium nitrate and water in accordance with ASTM D Standard 1505 Method B. The column was calibrated with glass floats of known density. Small pieces of film (ca. 25 mm^2) were placed in the column and allowed to equilibrate for 10 min before the measurements were taken. Averages of three measurements are reported in Table 1. The accuracy was $\pm 0.0009 \text{ g cm}^{-3}$.

The oxygen flux [$J(t)$] at 0% relative humidity, 1 atm, and 25 °C was measured with a Mocon Ox-Tran 2/20. Specimens were carefully conditioned as described previously⁴ to obtain the non-steady-state oxygen flux from which the diffusivity (D) was determined. The average thickness (l) of each specimen was determined from the measured density after the barrier measurement was completed.⁴ Most of the specimens were tested within 1–3 days of orientation. However, testing after 30 days produced the same flux curve and established that the specimens were fully relaxed.

Conformational composition was determined with photoacoustic Fourier transform infrared spectroscopy. Spectra were collected at ambient temperature with a Nicolet 870 Fourier transform infrared spectrometer with an MTEC model 200 photoacoustic cell. Specimens 10 mm in diameter were cut from the film after the barrier measurement. All infrared specimens were dried overnight *in vacuo* at ambient temperature for the removal of moisture. For each specimen, 256 scans were collected at a resolution of 4 cm^{-1} and a mirror velocity of 0.158 cm s^{-1} . The 1500–1400- cm^{-1} region of the spectrum was deconvoluted into three or four Gaussian peaks with Origin 4.1 software. The fractions of gauche and trans glycol configurations were obtained from the appropriate peak heights.

Table 1. Drawing Conditions and Physical Properties of Oriented Polyesters^a

Materials	Draw Ratio	<i>T</i> (°C)	Draw Rate (mm min ⁻¹)	Density (g cm ⁻³)	<i>P</i>	<i>D</i> × 10 ¹³	<i>S</i>	Trans Fraction	FFV
PEN	1.0	—	—	1.3280	0.167 ± 0.004	1.55 ± 0.04	0.125 ± 0.001	0.21	0.046
PEN	1.5	144	5	1.3290	0.162 ± 0.002	1.52 ± 0.03	0.123 ± 0.002	0.24	0.046
PEN	2.0	144	5	1.3300	0.157 ± 0.005	1.50 ± 0.02	0.122 ± 0.006	0.27	0.045
PEN	2.7	144	5	1.3371	0.097 ± 0.005	1.04 ± 0.02	0.108 ± 0.006	0.34	0.040
PEN	3.3	144	5	1.3440	0.059 ± 0.001	0.72 ± 0.01	0.095 ± 0.002	0.45	0.035
PEN	4.0	144	5	1.3495	0.038 ± 0.002	0.50 ± 0.02	0.088 ± 0.004	0.45	0.031
PEN	5.0	144	5	1.3511	0.032 ± 0.002	0.48 ± 0.03	0.077 ± 0.004	0.52	0.030
PEN	5.1	144	5	1.3532	0.027 ± 0.004	0.40 ± 0.02	0.078 ± 0.003	0.53	0.028
PEN	5.3	144	50	1.3540	0.026 ± 0.003	0.40 ± 0.04	0.074 ± 0.003	0.53	0.028
PEN	6.4	154	200	1.3560	0.020 ± 0.003	0.37 ± 0.01	0.064 ± 0.002	0.52	0.026
PET	1.0	—	—	1.3364	0.462	5.3	0.101	0.09	0.036
PET	2.1	70	5	1.3385	0.403	4.8	0.097	0.09	0.035
PET	2.6	80	20	1.3429	0.331	4.4	0.087	0.15	0.032
PET	3.1	70	5	1.3516	0.267	4.3	0.072	0.20	0.025
PET	3.1	80	50	1.3475	0.295	4.2	0.082	0.18	0.028
PET	3.8	70	5	1.3571	0.196	3.7	0.061	0.28	0.022
PET	4.0	60	5	1.3535	0.203	4.0	0.058	0.26	0.024
PET	4.0	70	5	1.3537	0.203	3.7	0.063	0.27	0.024
PET-BB55	1.0	—	—	1.3073	0.635 ± 0.004	6.4 ± 0.3	0.114 ± 0.005	0.07	0.040
PET-BB55/I5	1.0	—	—	1.3113	0.555 ± 0.011	5.4 ± 0.2	0.119 ± 0.001	0.09	0.038
PET-BB55/I10	1.0	—	—	1.3094	0.529 ± 0.015	5.1 ± 0.2	0.120 ± 0.002	0.09	0.039
PET-BB55	3.0	80	5	1.3250	0.315	4.5	0.081	0.23	0.027
PET-BB55/I5	3.0	64	5	1.3223	0.264 ± 0.005	4.3 ± 0.2	0.071 ± 0.002	0.19	0.029
PET-BB55/I5	3.4	74	5	1.3260	0.266 ± 0.010	4.4 ± 0.4	0.070 ± 0.003	0.24	0.027
PET-BB55	4.0	100	5	1.3354	0.147	3.1	0.055	0.39	0.020
PET-BB55	4.5	100	5	1.3371	0.106 ± 0.009	2.5 ± 0.2	0.049 ± 0.001	0.40	0.019
PET-BB55	6.0	100	50	1.3415	0.085	2.3	0.043	0.42	0.015
PET-BB55	6.5	100	50	1.3437	0.066 ± 0.001	2.4 ± 0.1	0.032 ± 0.002	0.44	0.014
PET-BB55/10I	7.0	100	50	1.3458	0.062 ± 0.001	1.8 ± 0.2	0.040 ± 0.001	0.49	0.012
PET-BB55	10.0	100	200	1.3490	0.060 ± 0.001	2.3 ± 0.1	0.030 ± 0.001	0.52	0.010
Vectra	—	—	—	1.3926	0.00055 ± 0.00018	0.17 ± 0.04	0.0038 ± 0.0010	—	—

^a *P* = permeability [cc(STP) cm m⁻² day⁻¹ atm⁻¹]; *D* = diffusivity (m² s⁻¹); *S* = solubility [cc(STP) cm⁻³ atm⁻¹].

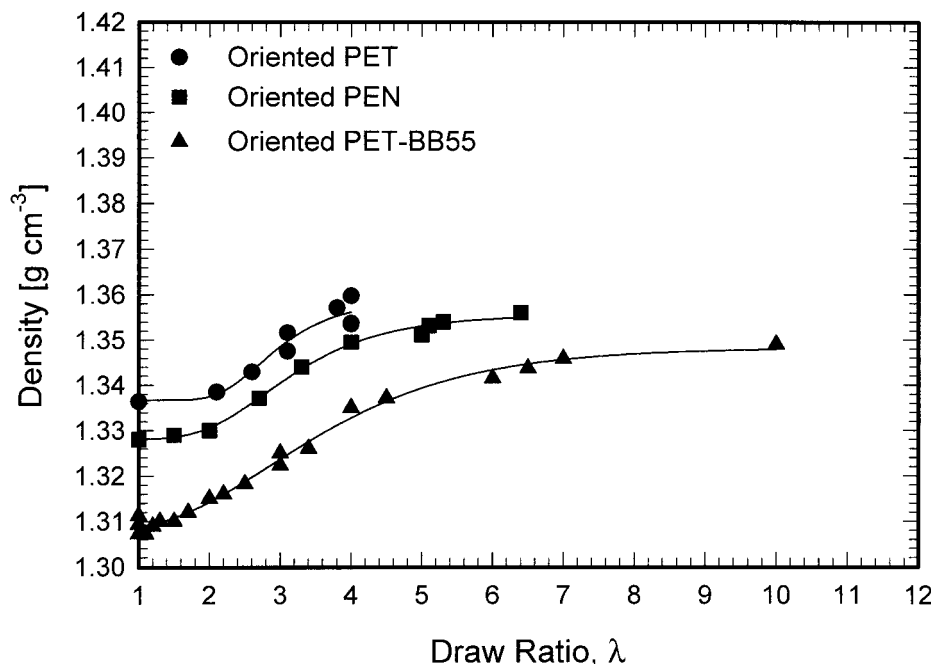


Figure 1. Relationship between the draw ratio and density for cold-drawn PET, PEN, and PET-BB55.

RESULTS

Oxygen Barrier of Oriented Polymers

A fairly narrow window in stretching conditions was available for achieving uniform extension of the polyesters without crystallization or stress whitening.⁶ Drawing at higher temperatures or slower rates resulted in crystallization, whereas drawing at lower temperatures or faster rates resulted in cavitation and stress whitening. Most of the draw ratios in Table 1 were achieved with a relatively slow draw rate at a draw temperature close to T_g . However, the highest draw ratios were obtained with both the draw rate and draw temperature increasing.

Increasing the draw ratio resulted in higher density. The nonlinear relationship between the density and draw ratio is shown in Figure 1. With PET, the highest draw ratio obtained with constrained uniaxial stretching was 4.0. Attempts to reach a higher draw ratio with an increasing draw rate resulted in stress whitening. The highest draw ratio obtained with PEN was 6.4. However, the density started to level off after the draw ratio reached approximately 4. The density of oriented PET-BB55 also began to level off after a draw ratio of 4–5, although a draw ratio as high

as 10 was obtained with this polymer. A high draw ratio without a corresponding increase in density suggested that chain slippage rather than chain extension dominated above a draw ratio of about 4.⁶ Lower entanglement density of the more rigid polymer chains facilitated slippage of PEN and PET-BB55 with respect to PET.

Experimental $J(t)$ curves through films of cold-drawn PET, PEN, and PET-BB55 are shown in Figure 2. To facilitate comparisons among specimens that varied somewhat in thickness, we normalized the flux curves to a film thickness of 200 μm . Careful conditioning and the appropriate choice of specimen thickness resulted in excellent resolution of the various features of the time dependence. The initial increase in oxygen flux reflected non-steady-state diffusion. This part of the curve was controlled mainly by the diffusivity (D). As the permeant concentration in the specimen reached a constant distribution, the flux reached the steady-state value (J_0). This value, normalized to both the film thickness (l) and the permeant gas pressure (p), defined the permeability ($P = J_0 l/p$).

To obtain D and accurately determine P , we fit the data to the solution of Fick's second law with appropriate boundary conditions:⁴

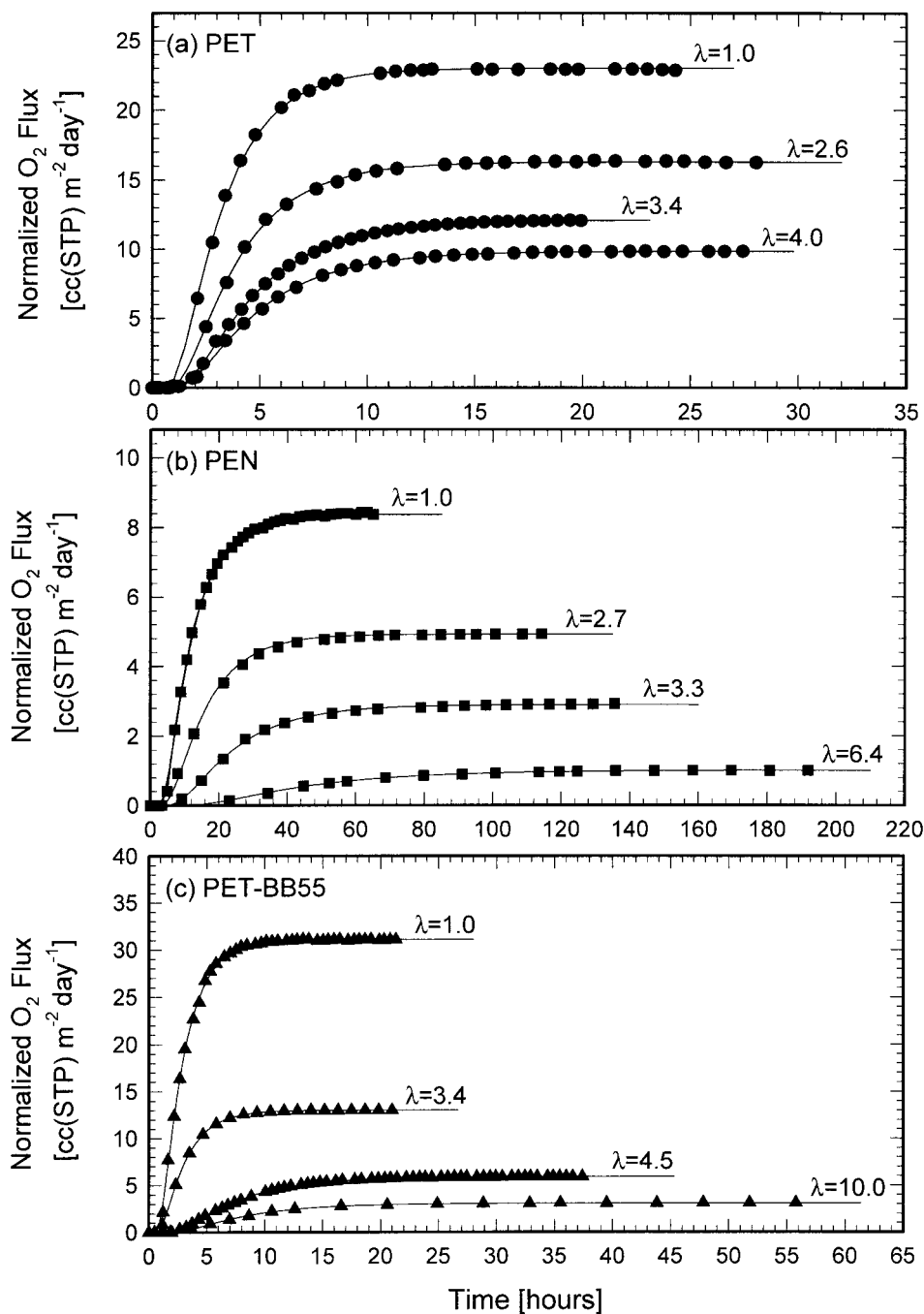


Figure 2. Experimental oxygen-flux data and fit to eq 1 (solid lines): (a) PET, (b) PEN, and (c) PET-BB55.

$$J(t) = \frac{Pp}{l} \left[1 + 2 \sum_{n=1}^{\infty} (-1)^n \exp\left(-\frac{D\pi^2 n^2 t}{l^2}\right) \right] \quad (1)$$

As indicated previously, the error in determining the two fitting parameters, P/l and D/l^2 , was estimated not to exceed 2%. The low sensitivity of

the diffusion flux to thickness variation within 30% was demonstrated previously.⁴ Therefore, the accuracy of P and D was determined mainly by the accuracy of the average thickness measurement. The bulk density method for determining the average film thickness was described previously.⁴

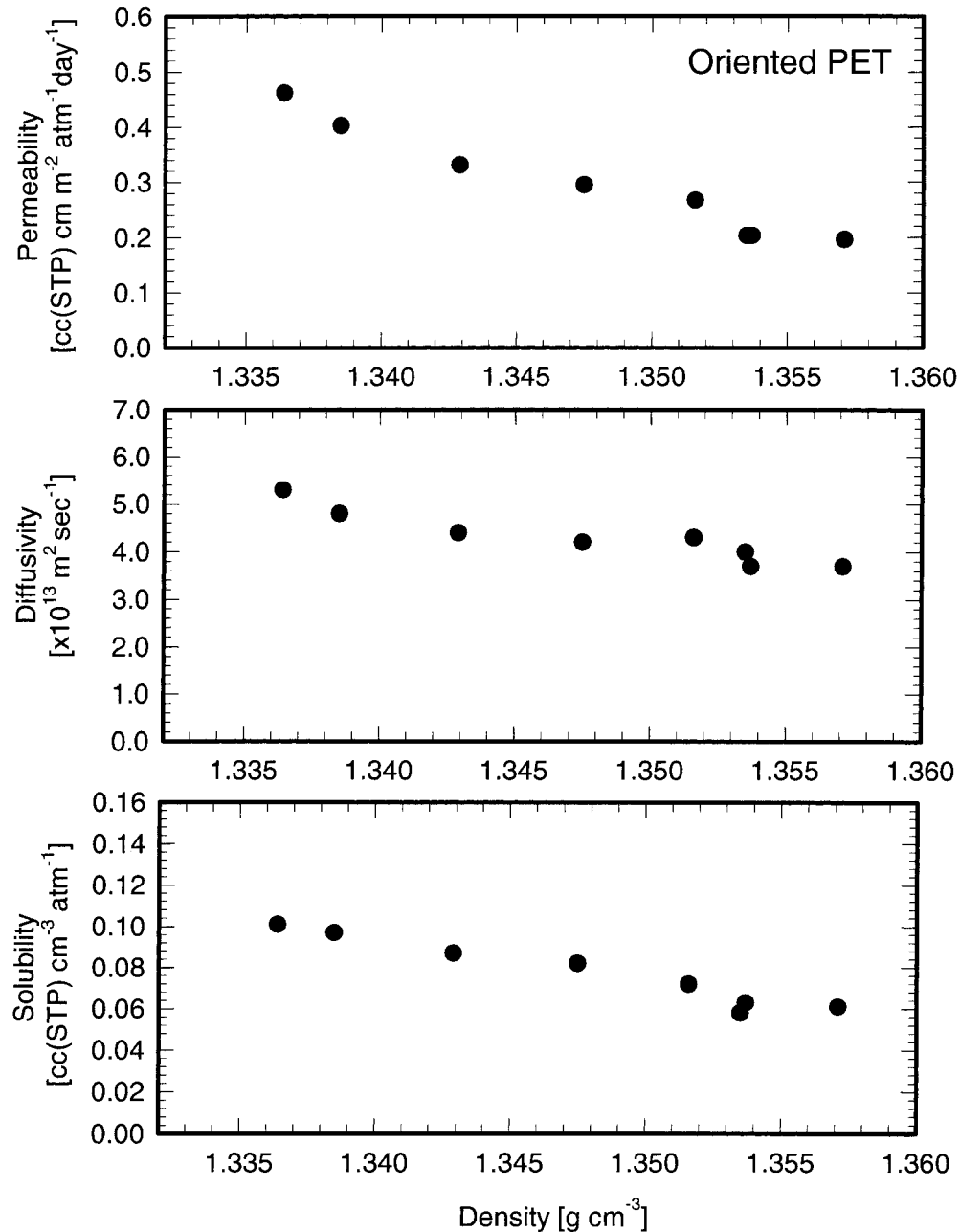


Figure 3. Effect of orientation (as density) on the oxygen-transport parameters of PET: (a) permeability, (b) diffusivity, and (c) solubility.

Cold drawing affected both the non-steady-state and steady-state parts of the oxygen-flux curve. The non-steady-state region broadened (slower diffusion), and the flux decreased (lower permeability). The oxygen flux was described well by the solution to Fick's second law as shown by the curve fits. Close agreement with the experimental data indicated that there was no concen-

tration dependence of oxygen diffusivity. Permeability and diffusivity, therefore, could be obtained from the fit accurately. Solubility (S) was calculated from the relationship $S = PD^{-1}$.

The effect of cold drawing on oxygen-barrier properties is shown in Figures 3–5, with the amount of orientation expressed in terms of the density. The highest orientation of PET de-

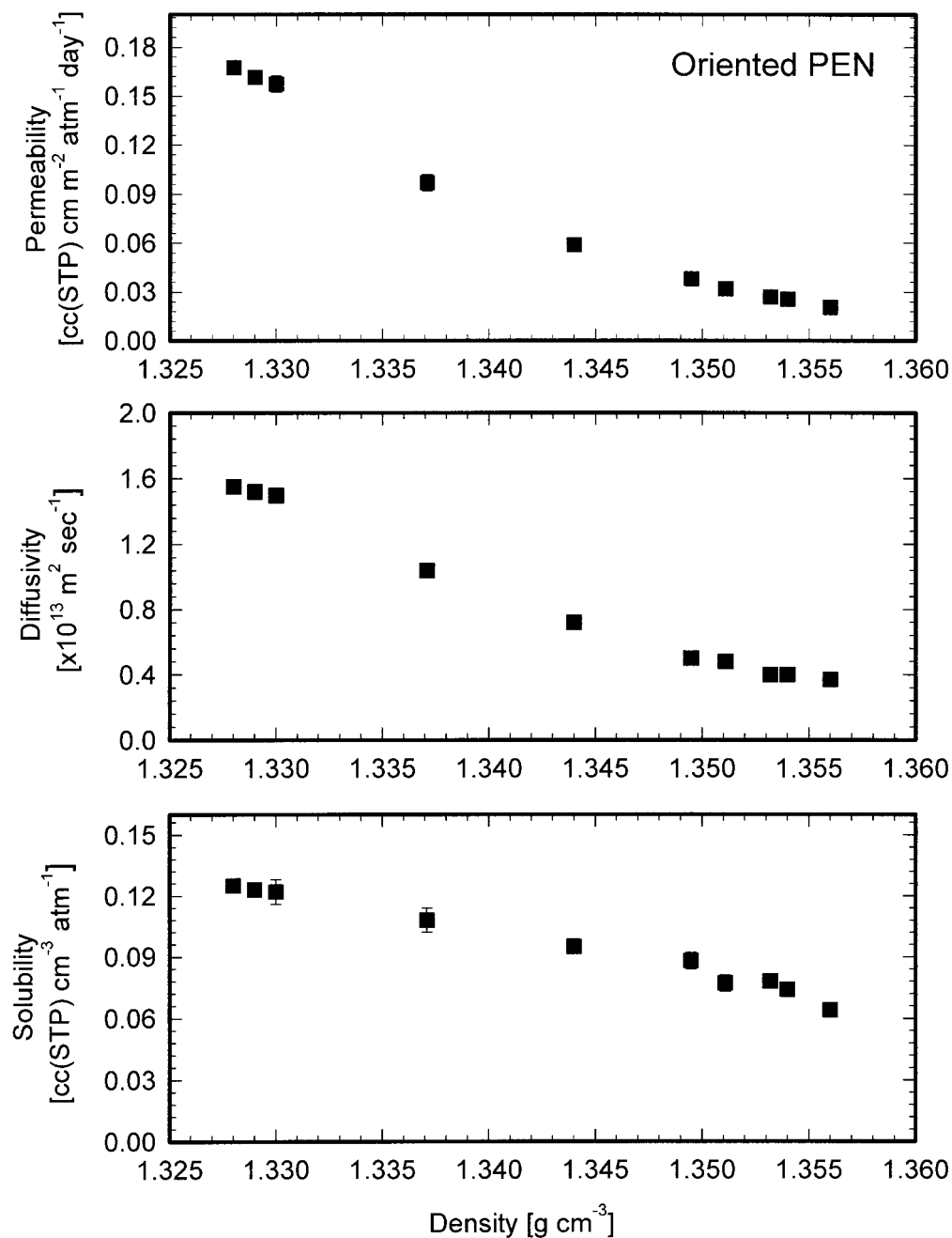


Figure 4. Effect of orientation (as density) on the oxygen-transport parameters of PEN: (a) permeability, (b) diffusivity, and (c) solubility.

creased the permeability by a factor of 2.3, from 0.462 to 0.203 cc(STP) cm m⁻² day⁻¹ atm⁻¹ (Table 1). This was due to decreases in both D and S . Without orientation, PEN had much lower permeability than PET [0.167 vs 0.462 cc(STP) cm m⁻² day⁻¹ atm⁻¹]. Moreover, the relative decrease in permeability achieved with orientation was larger. The highest orientation

reduced the permeability by a factor of 8, to 0.020 cc(STP) cm m⁻² day⁻¹ atm⁻¹. This decrease was mainly due to a large decrease in D . Although PET-BB55 had the highest permeability of the unoriented polymers [0.635 cc(STP) cm m⁻² day⁻¹ atm⁻¹], PET-BB55 exhibited the largest relative decrease with orientation. The highest orientation of PET-BB55

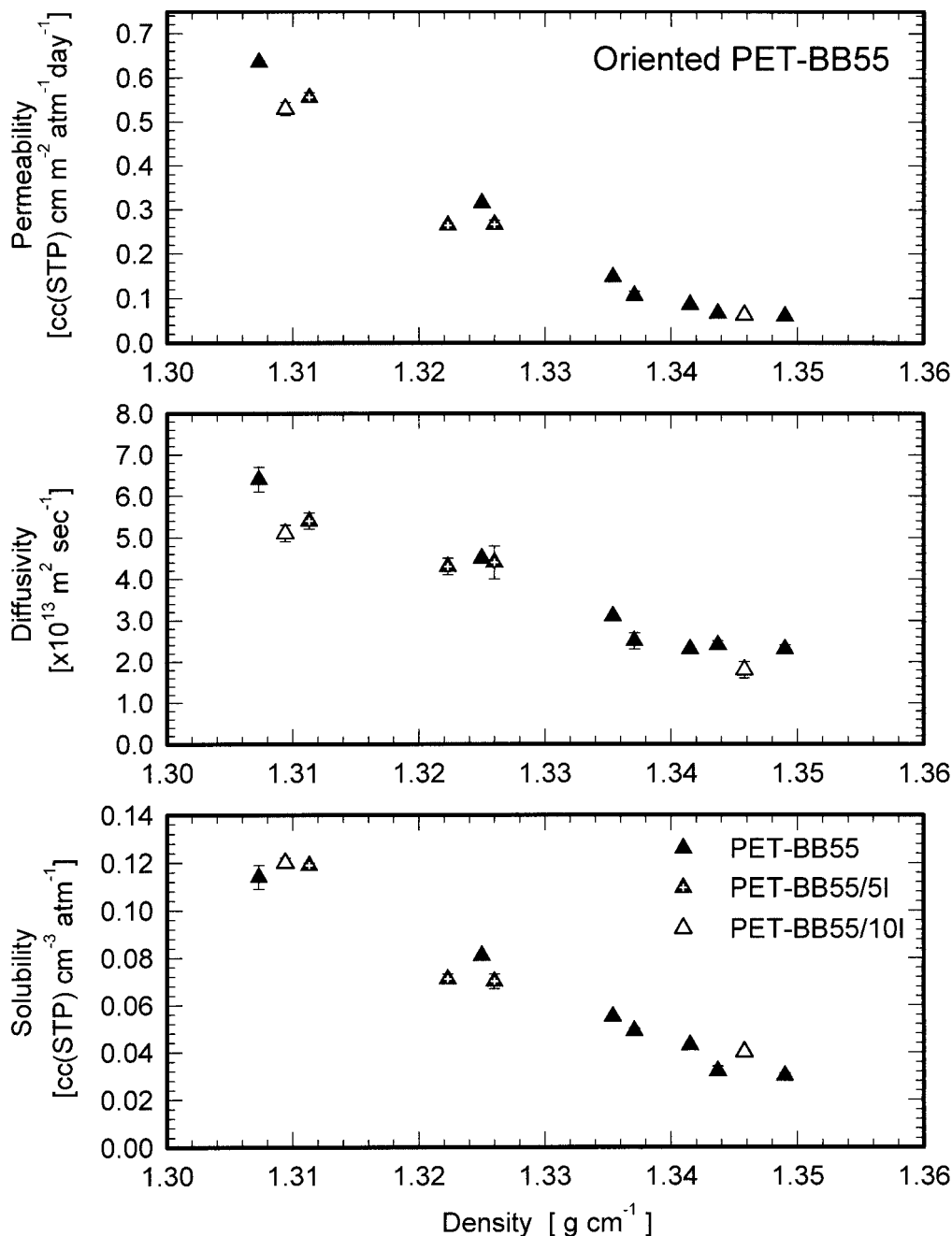


Figure 5. Effect of orientation (as density) on the oxygen-transport parameters of PET-BB55: (a) permeability, (b) diffusivity, and (c) solubility.

reduced the permeability by a factor of 10, to 0.060 cc(STP) cm m⁻² day⁻¹ atm⁻¹. This was due to large decreases in both D and S . Substituting 5 or 10% terephthalate with isophthalate in PET-BB55 to retard crystallization had no significant effect on the oxygen-transport parameters.

Conformer Characterization

The infrared spectra of PET⁷⁻⁹ and PEN¹⁰⁻¹² are well characterized. The glycol regions of the PET-BB55 spectrum closely resembled those of PET, and band assignments for PET-BB55 were made accordingly. Specific bands assigned to trans and

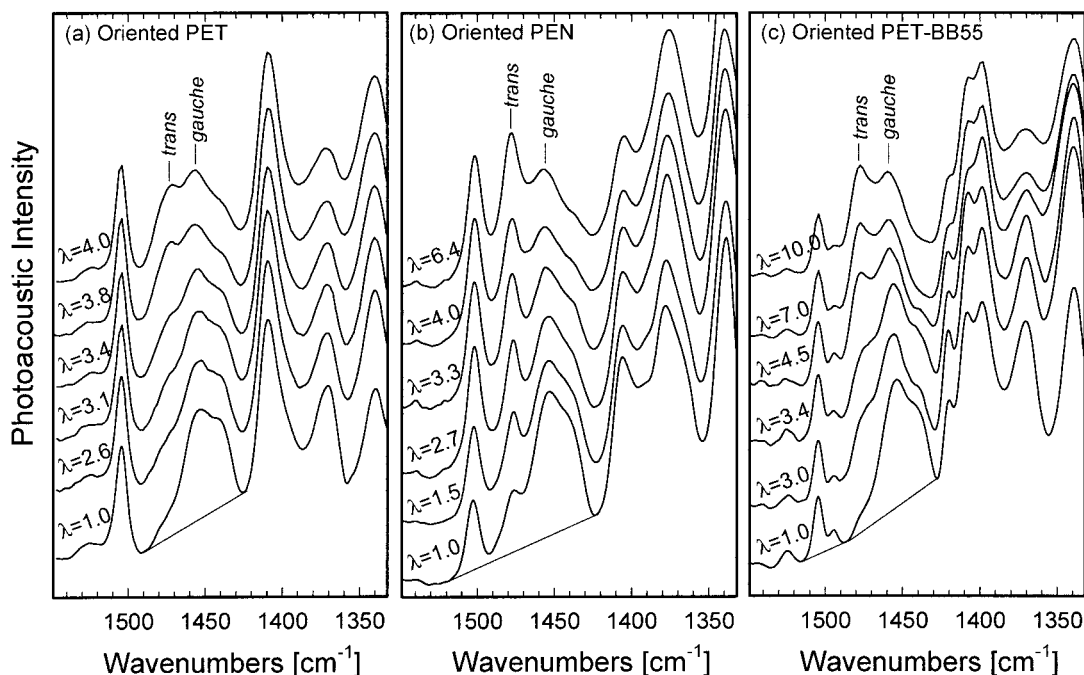


Figure 6. Effect of draw ratio λ on the 1500–1300- cm^{-1} region of the infrared spectrum: (a) PET, (b) PEN, and (c) PET-BB55.

gauche conformers of the PET and PEN glycol appear in three regions of the spectrum: 1500–1400, 1400–1300, and 1000–800 cm^{-1} . Changes in peak intensities in all three regions of the PET spectrum revealed the expected increase in trans conformers relative to gauche conformers with orientation. This is illustrated with the 1500–1400- and 1400–1300- cm^{-1} regions in Figure 6. Similar changes occurred in the spectrum of PET-BB55. However, the gauche band in the 1400–1300- cm^{-1} region of the PEN spectrum did not decrease with increasing trans content as expected, possibly because of an overlapping trans band.¹⁰ For this reason, the 1500–1400- cm^{-1} region was used for quantitative determination of conformer populations.

Spectra were normalized to the ester band at about 1730 cm^{-1} ,¹³ and the 1500–1400- cm^{-1} region was deconvoluted into three or four Gaussian peaks, as illustrated in Figure 7. The peak position was a variable in the deconvolution, but the frequencies of the gauche and trans bands obtained from the best fit did not shift with orientation by more than $\pm 1 \text{ cm}^{-1}$.

The relative amounts of gauche and trans conformers were determined by the plotting of the normalized peak heights, as in Figure 8. Excellent linearity was obtained for all the polymers.

Coincidence of the data for PET and PET-BB55 was consistent with the similarity in many features of their infrared spectra. The relationship was displaced for PEN but had the same slope, suggesting that the intensity of the reference band was somewhat different for PEN. Linear extrapolation gave intercepts that corresponded to the normalized band intensities for 100% trans and 100% gauche conformers, respectively.^{3,7} The gauche and trans bands used in the analysis had comparable absorbances.

The relationship between the density and trans fraction (f_{trans}), defined as

$$f_{\text{trans}} = \frac{\text{Normalized } 1476\text{-cm}^{-1} \text{ Peak Height}}{\text{Normalized } 1476\text{-cm}^{-1} \text{ Peak Height for 100\% Trans}}$$

is plotted in Figure 9. Without orientation, PET had a trans fraction of about 0.10, which agreed with the determinations of previous investigators who used other regions of the spectrum.^{3,14–16} The PET-BB55 copolymer had a similar trans fraction of about 0.08. In contrast, the trans fraction of PEN was larger, about 0.20, suggesting a more extended chain configuration. The trans fraction increased linearly with orientation, as

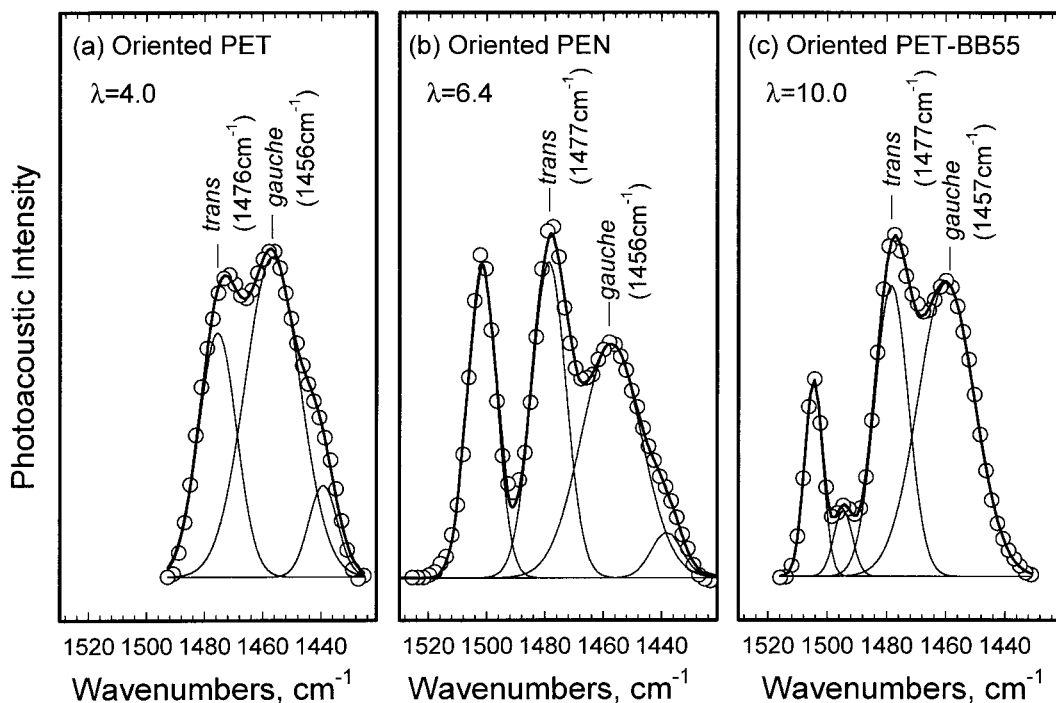


Figure 7. Examples showing the deconvolution of the 1500–1400-cm⁻¹ region of the infrared spectrum for peak heights of trans and gauche bands: (a) PET with $\lambda = 4.0$, (b) PEN with $\lambda = 6.4$, and (c) PET-BB55 with $\lambda = 10.0$.

measured by density. Similarity in the slopes of the relationship indicated that the incremental increase in density accompanying the gauche-to-trans transformation was the same for the three polymers. However, a larger increase in the trans fraction was achieved by the cold drawing of PET-BB55 (0.08–0.50) than by the cold drawing of PET (0.10–0.30) or PEN (0.20–0.50). Extrapolation of the linear relationship provided the density of the glass with all gauche conformers and the glass with all trans conformers (Table 2). Very similar values were reported previously for the amorphous densities of gauche and trans PET.⁸ Significantly higher glass densities for PET than for PEN indicated more efficient packing, whereas the extrapolated glass densities of PEN and PET-BB55 were virtually the same.

DISCUSSION

Recognition of an additivity relationship between the density and trans fraction of cold-drawn PET previously motivated the formulation of a two-phase permeability model consisting of a permeable amorphous phase with ethylene linkages

predominately in the gauche conformation and an impermeable amorphous phase with ethylene linkages that had transformed from the gauche conformation to the trans conformation during stretching.³ The two-phase model was particularly useful for describing the effects of heat setting after orientation.

Results of the more extensive study described here, which extends to other aromatic polyesters, confirm the linear relationship between the density and trans fraction and are, therefore, amenable to interpretation in terms of the two-phase model. However, an alternative interpretation of the oriented glass is possible, one that is based on a single phase. The one-phase approach permits an interpretation of orientation that is consistent with previously established free-volume concepts of polymer glasses.

Free volume is a useful molecular-scale concept for interpreting transport properties.¹⁷ The permeation of small gas molecules through a glassy polymer is viewed as proceeding by a jumping mechanism whereby a penetrant molecule spends most of its time in free-volume cavities and occasionally jumps into a neighboring cavity. Gas permeation depends on the number and size of cav-

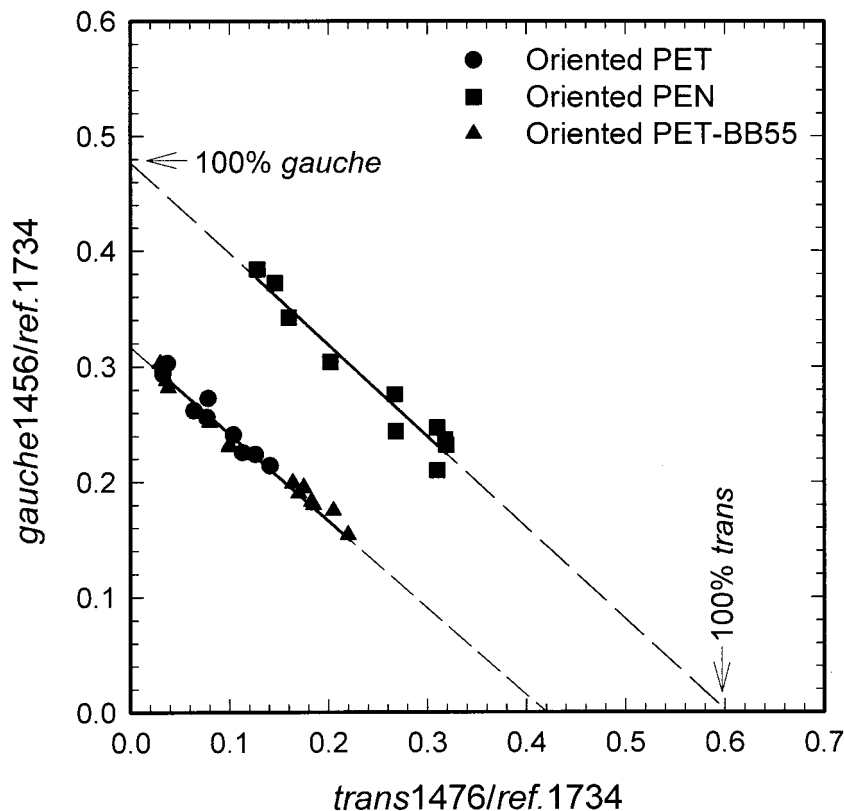


Figure 8. Normalized peak heights of the gauche and trans infrared bands.

ities (static free volume) and the frequency of jumps (dynamic free volume). Studies of glassy polyesters based on PET demonstrate that oxygen sorption at 1 atm is the process of filling holes of static free volume, and the solubility is proportional to the amount of free volume.^{14,18}

Figure 10 shows the solubility plotted against the specific volume of oriented PET, PEN, and PET-BB55. The solid line, with a slope (β) of $3.6 \text{ cc(STP) g cm}^{-6} \text{ atm}^{-1}$ and an extrapolated zero-solubility specific volume (ν_0) of $0.721 \text{ cm}^3 \text{ g}^{-1}$, was taken from previous publications in which a single linear relationship between the oxygen solubility and polymer specific volume described many amorphous PET-based copolymers^{14,18} and also described the dedensified amorphous phase of crystallized PET.^{4,19} The oxygen solubility of cold-drawn PET followed the same relationship. The correlation suggested that cold-drawn PET could be regarded as a one-phase densified glass. Similarly, a linear relationship between the solubility and specific volume was observed for PEN and PET-BB55.

The extrapolated zero-solubility specific volume was much larger for PET-BB55 than for PET

and PEN (Table 2). However, the slope of the oxygen solubility versus the specific volume was virtually the same for all three polymers. It reflected the density of sorbed oxygen (d), which was extracted from β as

$$d = \nu\beta P \left(\frac{M_w}{22,400} \right) \quad (2)$$

where ν is the specific volume of the glassy polymer, $P = 1 \text{ atm}$ is the ambient pressure of oxygen gas, and $M_w = 32$ is the weight-average molecular weight for oxygen. The density of sorbed oxygen, $3.9 \times 10^{-3} \text{ g per cm}^3$ of free volume or about 3 atm, indicated that the sorbed oxygen was in the gaseous state. An experimental demonstration that the gas density was virtually the same in PET, PEN, and PET-BB55 validated the assumption, made in a previous publication,¹⁸ that the chemical structure of glassy polyesters affected ν_0 but not β .

From the proportionality between the solubility and amount of accessible free volume,^{14,18} the specific accessible free volume (ν_f) can be obtained from β as

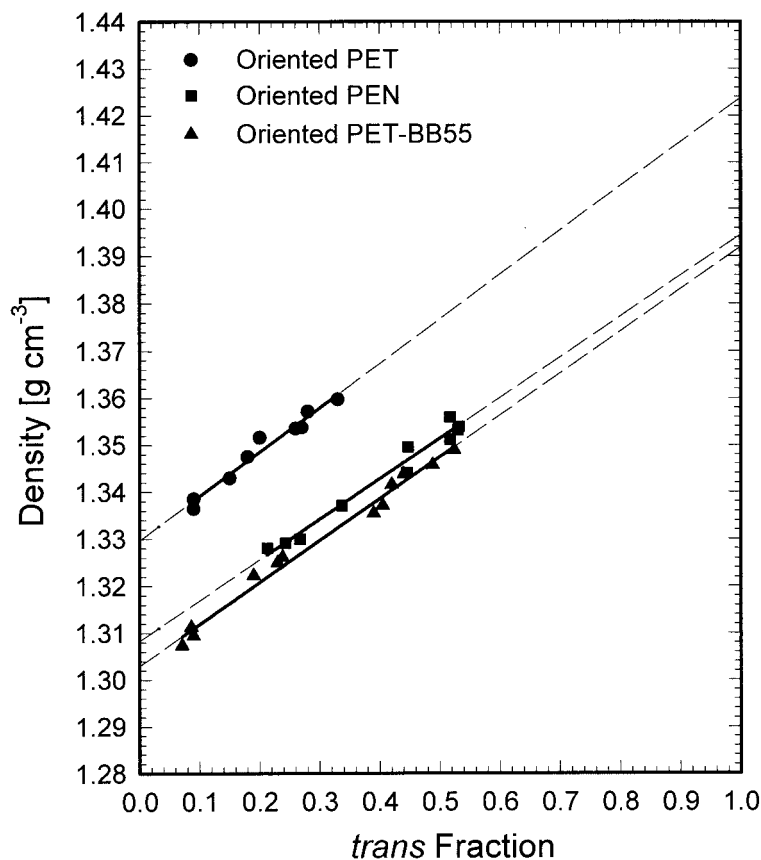


Figure 9. Relationship between the density and trans fraction for cold-drawn PET, PEN, and PET-BB55.

$$\nu_f = \nu - \nu_0 = \frac{S}{\beta} \quad (3)$$

The fractional free volume (FFV) given in Table 1 is

$$\text{FFV} = \frac{\nu - \nu_0}{\nu} = \frac{S}{\beta\nu} \quad (4)$$

where ν is the specific volume obtained from the measured density and ν_0 is the extrapolated specific volume at zero solubility. Therefore, a constant value of β indicates a fundamental similarity in the characteristics of the accessible free volume in glassy polyesters, whereas ν_0 reflects a characteristic of the chemical structure.

Because of the long timescale required for glassy polymers to relax fully, gas transport typ-

Table 2. Characteristics of Amorphous Polyesters at 25 °C

Property	PET	PEN	PET-BB55
Slope β [cc(STP) g cm ⁻⁶ atm ⁻¹]	3.6 ± 0.1	3.6 ± 0.1	3.7 ± 0.1
Sorbed O ₂ density (10 ⁻³ g cm ⁻³)	3.9 ± 0.1	3.9 ± 0.1	4.0 ± 0.1
Sorbed O ₂ pressure (atm)	3.0 ± 0.1	3.0 ± 0.1	3.1 ± 0.1
Density of trans conformers (g cm ⁻³)	1.423 ± 0.010	1.394 ± 0.010	1.392 ± 0.010
Density of gauche conformers (g cm ⁻³)	1.330 ± 0.002	1.308 ± 0.004	1.303 ± 0.002
Density at zero solubility (g cm ⁻³)	1.387 ± 0.009	1.393 ± 0.005	1.361 ± 0.007
Trans fraction at zero solubility	0.61 ± 0.10	0.99 ± 0.06	0.65 ± 0.08

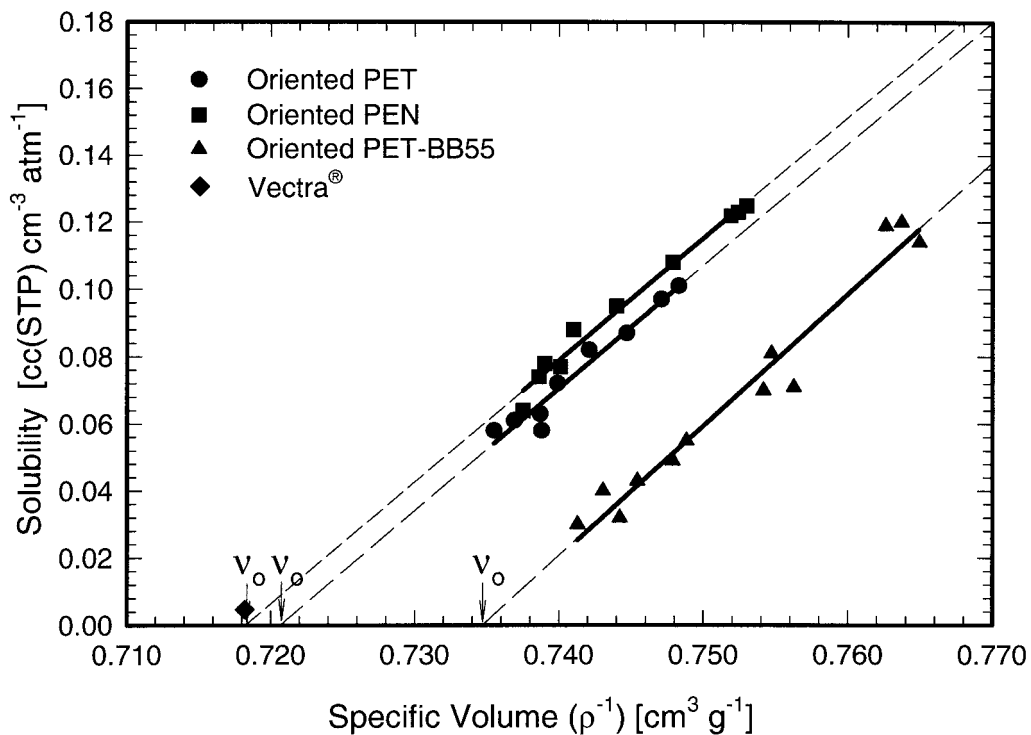


Figure 10. Relationship between the oxygen solubility and specific volume ($\nu = \rho^{-1}$).

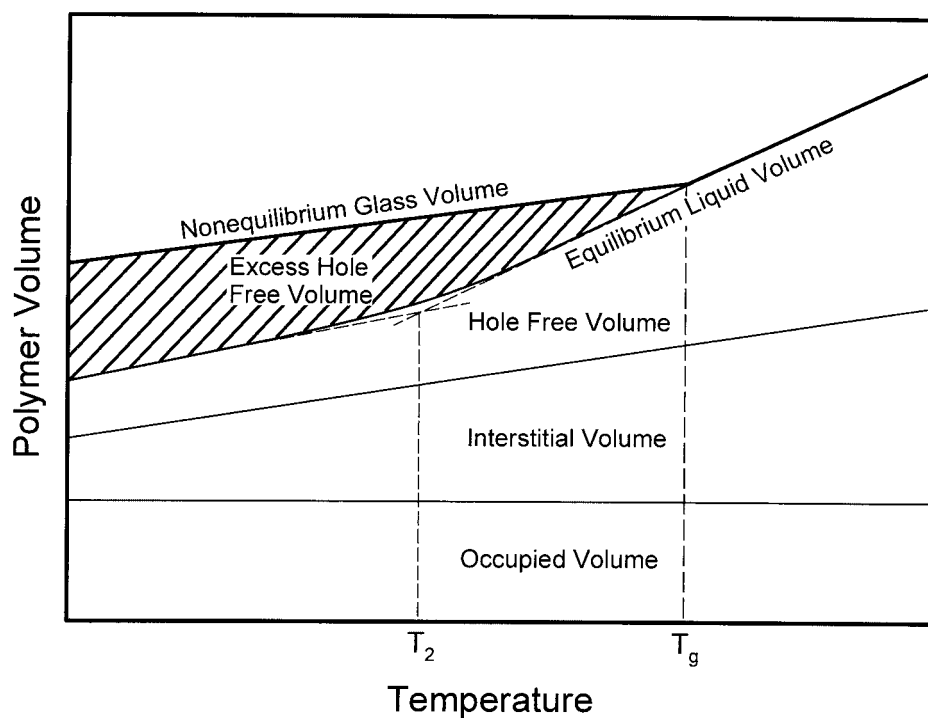


Figure 11. Schematic representation of the volume–temperature relationship for an amorphous polymer following the concepts of Vrentas and Duda.²⁰

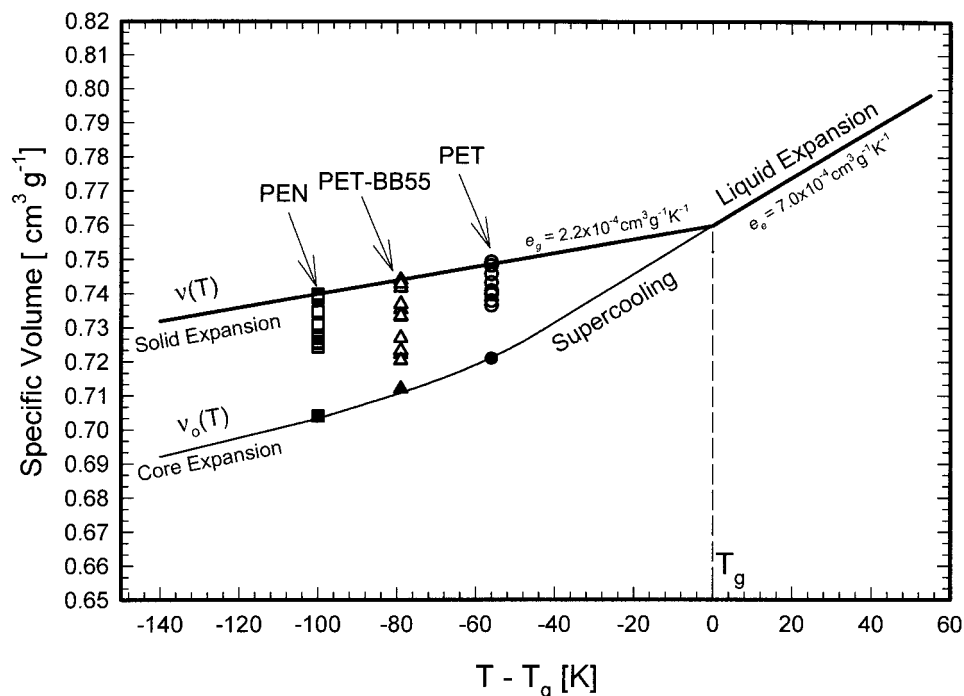


Figure 12. Specific volume–temperature relationship constructed for amorphous PET with oxygen solubility as a measure of accessible free volume and including the effect of orientation.

ically occurs under nonequilibrium conditions wherein the polymer possesses more free volume than it would at equilibrium. According to the concepts of Vrentas and Duda,²⁰ the volume of the nonequilibrium glassy polymer is larger than the equilibrium volume extrapolated from the excess-hole free volume (Fig. 11). A previous study of copolymers based on PET demonstrates that the free volume accessible to oxygen gas correlates with the excess-hole free volume described in the Vrentas and Duda model.¹⁸ Therefore, ν_0 represents a point on the equilibrium curve.

Orientation by cold drawing is viewed as decreasing the excess-hole free volume and bringing the nonequilibrium polymer glass closer to the equilibrium line. The orientation effect is incorporated into the model by the construction of the volume–temperature relationship, as described previously.¹⁸ The plot in Figure 12 is constructed for PET. The specific volume of the quenched glass at 25 °C ($T - T_g = -56$ °C), taken together with the specific thermal expansivity, $2.2 \times 10^{-4} \text{ cm}^3 \text{ g}^{-1} \text{ K}^{-1}$ for the amorphous solid and $7.0 \times 10^{-4} \text{ cm}^3 \text{ g}^{-1} \text{ K}^{-1}$ for the liquid, define the $\nu(T)$ curve. The core expansion curve $\nu_0(T)$ is taken from a previous publication¹⁸ and is based on the specific excess-hole free volume, calculated from

the oxygen solubility, of many glassy polyesters. Additional points for oriented PET show how the specific volume approaches the equilibrium $\nu_0(T)$ curve with increasing orientation.

For the incorporation of PEN and PET-BB55 into the plot, the specific excess-hole free volume ν_f of the unoriented glass was calculated from eq 3 and subtracted from the amorphous glass line of PET at the appropriate value of $T - T_g$. This placed two additional points on the $\nu_0(T)$ curve. Consistent with the model (Fig. 11), the specific excess-hole free volume became less dependent on temperature and indeed appeared to approach a constant value around $0.04 \text{ cm}^3 \text{ g}^{-1}$ or an FFV of approximately 0.05. These values are in line with estimations of FFV in glassy polymers based on molecular dynamics simulations¹⁷ and group contributions.²¹

Similarly, the specific excess-hole free volume of the oriented glass was obtained from eq 3 and was subtracted from the specific excess-hole free volume of the unoriented glass to obtain $\Delta\nu_f$, which represented the free volume that was removed by cold drawing. The quantity $\Delta\nu_f$ was subtracted from the amorphous glass line to locate the effect of orientation on the volume–temperature relationship in Figure 12. The plot indi-

cated that cold-drawn PET-BB55 came closer to the equilibrium (zero-solubility) condition than cold-drawn PET or PEN.

Extremely low gas solubility is characteristic of liquid-crystalline polymers.²² Vectra film with oxygen solubility an order of magnitude lower than even the most highly oriented PET-BB55 illustrates this feature (Table 1). With a high percentage of naphthalate units, Vectra resembles PEN more closely than the other polymers in chemical structure. It is consistent that when plotted on Figure 10, the point for Vectra is close to ν_0 of PEN. The homopolymer, poly(ethylene terephthalate), is also reported to be liquid-crystalline.^{23–25} The PET-BB55 copolymer possibly possesses some liquid-crystalline-like character that can account for the high draw ratio achieved by cold drawing and the effectiveness of cold drawing in removing excess-hole free volume.

The conformer composition corresponding to the zero-solubility density ($\rho_0 = \nu_0^{-1}$) was obtained from Figure 9. For PEN, the density at zero solubility correlated with 100% trans conformers (Table 2). In contrast, the zero-solubility density of both PET and PET-BB55 matched a conformer population of only 60–65% trans conformers. A possible explanation can be derived from the coincidence of the slope change in the equilibrium glass line of Figure 12 with the postulated second-order transition at approximately $T_g - 60$ °C.^{26–28} By definition, the configurational entropy goes to zero at the transition temperature.²⁶ In this cases, all the glycol linkages should be in the trans conformation. At 25 °C, only PEN ($T_g = 128$ °C) is definitely below the transition temperature. Both PET ($T_g = 81$ °C) and PET-BB55 ($T_g = 104$ °C) are in the broad transition region in which the equilibrium glass can possess some fraction of gauche conformations. These gauche conformations could take the form of extended, noncrystallizable kinked conformers, which have been proposed as an alternative to the all-trans conformation in oriented amorphous PET.²⁹

CONCLUSIONS

Orientation is one approach to improving oxygen-barrier properties of polyesters. This study focused on the orientation of PET, PEN, and PET-BB55 by cold drawing. Decreases in both diffusivity and solubility contributed to lower permeability. Oxygen solubility in cold-drawn PET followed the linear

dependence on specific volume previously established for glassy copolymers of PET. This made it possible to view the oriented polymer as a one-phase glass and to consider the orientation process as decreasing the amount of excess-hole free volume. For the polymers studied, the zero-solubility condition was approached most closely with cold-drawn PET-BB55. The processes of orientation and densification by cold drawing were correlated with the conformational transformation of glycol linkages from gauche to trans. Complete transformation to trans conformers correlated with the exclusion of all excess-hole free volume (zero solubility) only for PEN.

The authors thank Dr. Liqun Zhang for fruitful discussions concerning this research. Financial support from the National Science Foundation (DMR 9975774 and DMR 9986467) and KoSa is gratefully acknowledged. Modern Controls, Inc., generously supported the development of a facility for gas-transport studies at Case Western Reserve University.

REFERENCES AND NOTES

- Slee, J. A.; Orchard, G. A. J.; Bower, D. I.; Ward, I. M. *J Polym Sci Part B: Polym Phys* 1989, 27, 71–83.
- Orchard, G. A. J.; Spiby, P.; Ward, I. M. *J Polym Sci Part B: Polym Phys* 1990, 28, 603–621.
- Qureshi, N.; Stepanov, E. V.; Schiraldi, D.; Hiltner, A.; Baer, E. *J Polym Sci Part B: Polym Phys* 2000, 38, 1679–1686.
- Sekelik, D. J.; Stepanov, S. V.; Nazarenko, S.; Schiraldi, D.; Hiltner, A.; Baer, E. *J Polym Sci Part B: Polym Phys* 1999, 37, 847–857.
- Armeniadis, C. D.; Baer, E. *J Polym Sci Part A-2: Polym Phys* 1971, 9, 1345–1369.
- Sun, N.; Yang, J.; Gu, Q.; Shen, D. *J Appl Polym Sci* 2000, 77, 2044–2048.
- Guèvremont, J.; Aiji, A.; Cole, K. C.; Dumoulin, M. M. *Polymer* 1995, 36, 3385–3392.
- Lin, S.-B.; Koenig, J. L. *J Polym Sci Polym Phys Ed* 1982, 20, 2277–2295.
- Walls, D. J. *Appl Spectrosc* 1991, 45, 1193–1198.
- Ouchi, I.; Hosoi, M.; Shimotsuma, S. *J Appl Polym Sci* 1977, 21, 3445–3456.
- Kimura, F.; Kimura, T.; Sugisaki, A.; Komatsu, M.; Sata, H.; Ito, E. *J Polym Sci Part B: Polym Phys* 1997, 35, 2741–2747.
- Vasanthan, N.; Salem, D. R. *Macromolecules* 1999, 32, 6319–6325.
- Cole, K. C.; Ben Daly, H.; Sanschagrin, B.; Nguyen, K. T.; Aiji, A. *Polymer* 1999, 40, 3505–3513.
- Polyakova, A.; Connor, D. M.; Collard, D. M.; Schiraldi, D. A.; Hiltner, A.; Baer, E. *J Polym Sci Part B: Polym Phys* 2001, 39, 1900–1910.

15. Ajji, A.; Guèvremont, J.; Cole, K. C.; Dumoulin, M. M. *Polymer* 1996, 37, 3707–3714.
16. Ajji, A.; Cole, K. C.; Dumoulin, M. M.; Brisson, J. *Polymer* 1995, 36, 4023–4030.
17. Theodorou, D. N. In *Diffusion in Polymers*; Neogi, P., Ed.; Marcel Dekker: New York, 1996; Chapter 2, pp 67–142.
18. Polyakova, A.; Liu, R. Y. F.; Schiraldi, D. A.; Hiltner, A.; Baer, E. *J Polym Sci Part B: Polym Phys* 2001, 39, 1889–1899.
19. Polyakova, A.; Stepanov, E. V.; Sekelik, D.; Schiraldi, D. A.; Hiltner, A.; Baer, E. *J Polym Sci Part B: Polym Phys* 2001, 39, 1911–1919.
20. Vrentas, J. S.; Duda, J. L. *J Appl Polym Sci* 1978, 22, 2325–2339.
21. Park, J. Y.; Paul, D. R. *J Membr Sci* 1997, 125, 23–39.
22. Chiou, J. S.; Paul, D. R. *J Polym Sci: Part B: Polym Phys* 1987, 25, 1699–1707.
23. Li, X.; Brisse, F. *Macromolecules* 1994, 27, 2276–2282.
24. Krigbaum, W. R.; Asrar, J.; Toriumi, H.; Ciferri, A.; Preston, J. *J Polym Sci Polym Lett Ed* 1982, 20, 109–115.
25. Meurisse, P.; Noël, C.; Monnerie, L.; Fayolle, B. *Br Polym J* 1981, 13, 55–63.
26. Gibbs, J. H.; DiMarzio, E. A. *J Chem Phys* 1958, 28, 373–383.
27. Miller, A. A. *J Polym Sci Part A: Gen Pap* 1963, 1, 1857–1863.
28. Miller, A. A. *J Polym Sci Part A: Gen Pap* 1963, 1, 1865–1874.
29. Tonelli, A. E. *Polymer* 2002, 43, 637–642.